Confocal Raman Observation of the Efflorescence/Deliquescence Processes of Individual $NaNO_3$ Particles on Quartz

Xiao-Hong Li, Feng Wang, Pei-Dong Lu, Jin-Ling Dong, Liang-Yu Wang, and Yun-Hong Zhang*

The Institute for Chemical Physics, Beijing Institute of Technology, Beijing, China 100081

Received: July 5, 2006; In Final Form: October 15, 2006

Confocal Raman spectroscopy was used to study the structural changes of bulk $NaNO_3$ solutions with molar water-to-solute ratios (WSRs) of 54.0−12.3 and $NaNO_3$ droplets (10−100 μm) with WSRs of 9.5−1.0 on a quartz substrate. Upon reduction of the WSR, a blue shift of the symmetric stretching band ($\nu_1(NO_3^-)$) from ∼1048 to ∼1058 cm^{-1} was observed in the confocal Raman spectra with high signal-to-noise ratios. Accordingly, the full width at half-height of the $\nu_1(NO_3^-)$ band increased from ∼8.4 cm^{-1} for the dilute solution (WSR = 54.0) to ∼15.6 cm^{-1} for the extremely supersaturated droplet (WSR = 1.0), suggesting the formation of contact ion pairs with different structures. For the O−H stretching band, the ratio of weak hydrogen-bonding components to strong ones, i.e., I_{3488}/I_{3256}, increased from ∼1.2 at WSR = 54.0 to ∼7.3 at WSR = 1.0, indicating that the strong hydrogen bonds were heavily destroyed between water molecules especially in the supersaturated droplets. In the humidifying process, two hygroscopic behaviors were observed depending on the morphology of solid $NaNO_3$ particles. No surface water was detected for a solid $NaNO_3$ particle with rhombohedral shape at relative humidities (RHs) below 86%. When the RH increased from 86% to 93%, it suddenly absorbed water and turned into a solution droplet. For a maple-leaf-shaped $NaNO_3$ particle with a rough surface, however, a trace of residual water originally remained on the rough surface even at very low RH according to its Raman spectrum. Its initial water uptake from the ambient occurred at ∼70% RH. The small amount of initially adsorbed water induced surface rearrangement of the maple-leaf-shaped particle. A further increase of RH made the particle gradually turn into a regular solid core swathed in a solution layer. Eventually, it completely deliquesced in the RH region of 86−93%, similar to the case of the $NaNO_3$ particle with rhombohedral shape.

Introduction

Metastable supersaturated aerosols commonly exist in atmosphere due to the suppression of both heterogeneous and homogeneous nucleation in the tiny aerosol droplets.[1,2] Thus, contact ion pairs (CIPs) can be probed more easily in the supersaturated aerosols where the molar water-to-solute ratio (WSR) is too low to satisfy a full hydration layer both for anions and for cations. How to understand the CIPs on the molecular level is a focus of atmospheric science, solution chemistry, and life science.[3−6] The electrodynamic balance (EDB) can levitate individual droplets and has been successfully used to study the supersaturated droplets. With the combination of the EDB technique and Raman spectroscopy, the structures of supersaturated sulfate,[7,8] perchlorate,[9] acetate,[10] and nitrate[11,12] droplets have been deeply investigated on the molecular level. Other levitation techniques, such as optical levitation[13−16] and sonic levitation,[17] were used to study dynamic processes and chemical reactions of droplets. For a perfect spherical droplet, however, a lot of strong Mie scattering lines from the morphology-dependent resonances (MDRs) usually overlapped with the Raman bands. To acquire Raman spectra about the chemical information of contact ion pairs, we had to measure over 50 Raman spectra at a given relative humidity (RH) and obtained the average from those without contribution of physical MDRs.[7,8,11] In addition, the MDRs strongly distorted the O−H stretching band in the Raman spectra, which limited the investigation of the hydrogen-bonding structures between water molecules.[8]

Every year, as much as 10^{12} kg of sea salt is introduced into the atmosphere by breaking waves and bursting bubbles on the ocean surface, which is one of the main sources of the atmospheric aerosols.[18−21] Sodium chloride, which is abundant in sea salt, commonly reacts with the trace oxides of nitrogen, including NO_2, HNO_3, N_2O_5, and $ClONO_2$, to produce sodium nitrate.[20] As one of the principal components of aged sea salt aerosols in the atmosphere, sodium nitrate has much relation to the human environment. It eventually returns to the ground by precipitation (e.g., rainfall), contributing to nitrogen saturation in the coastal ecosystem. The physical states of $NaNO_3$ particles severely influence the radiative properties of the marine boundary layer.[20] Though many researchers paid attention to the phase transitions of sodium nitrate particles, there was no agreement on their hygroscopic properties.[2,22−27] In the dehumidifying process, Tang et al. observed that the single $NaNO_3$ droplets levitated in the EDB cell effloresced in the RH range 35−0.05% by means of the EDB technique.[12,24] However, Gysel et al. discovered the micrometer-sized $NaNO_3$ droplets did not crystallize even at 6% RH by use of the hygroscopicity tandem differential mobility analyzer (H-TDMA) method.[26] In the humidifying process, Tang et al. observed a deliquescence point of 74.5% RH (at 25 °C) for the levitated solid $NaNO_3$ particle.[12,24] However, no distinct deliquescence point was observed in other studies.[25−27] For example, Lee and

* To whom correspondence should be addressed. Phone: 86-10-86668406. Fax: 86-10-68912652. E-mail: yhz@bit.edu.cn.

10.1021/jp064221o CCC: $33.50
Published on Web 11/21/2006

Hsu observed that water uptake of the $NaNO_3$ aerosols was a continuous process in a wide RH range of 25−89%.[25] Using the TDMA technique, Gysel et al. measured growth factors of $NaNO_3$ particles at 20 and −10 °C with increasing RH from 6% to 95%.[26] They found that the $NaNO_3$ particles did not exhibit the deliquescence phenomenon. Hoffman et al. also did not observe the deliquescence point of $NaNO_3$ aerosol particles although they used several approaches.[27]

Even though the $NaNO_3$ droplets were found not to effloresce even at 6% RH,[26] there was no detailed understanding on the interactions between Na^+ and NO_3^- and the hydrogen bonds between water molecules in the supersaturated $NaNO_3$ droplets. We have tried to study the supersaturated $NaNO_3$ droplets by the EDB−Raman method, but no significant information was obtained due to the strong disturbance of the MDRs on the Raman spectra.

Very recently, the supersaturated state was proved to be easily achieved for the droplets deposited on a quartz substrate through simply decreasing their ambient RH.[28] This kind of droplet can provide Raman spectra without MDR disturbance due to their half-ellipsoidal shape. In this work, we try to obtain high signal-to-noise (S/N) ratio Raman spectra of the $NaNO_3$ droplets at various RHs with the confocal Raman technique. According to the evolution of the symmetric stretching band of NO_3^- ($\nu_1(NO_3^-)$), we intend to draw out the structural information on the complicated contact ion pairs in the supersaturated $NaNO_3$ droplets. On the basis of the water stretching vibration band ($\nu(H_2O)$), we also expect to understand the hydrogen bonds between water molecules in the supersaturated state. By preparing the solid $NaNO_3$ particles with different shapes, we look forward to understanding the dependence of the deliquescence process on particle morphology.

Experimental Section

Sample Preparation. Bulk $NaNO_3$ solutions with different WSRs were prepared by dissolving analytical-grade sodium nitrate in triply distilled water without further purification. By use of a syringe, $NaNO_3$ droplets (10−100 μm) were injected onto a quartz substrate fixed to the bottom of the sample chamber. The sample chamber was sealed with a thin transparent polyethylene (PE) film and mounted on the automated motorized stage attached to the Raman spectroscopy system. To increase the S/N ratio, droplets with larger diameters were selected first to acquire the Raman spectra. Smaller droplets had to be selected to get the spectra at low RHs, where the droplets with larger sizes had already crystallized. The RH in the chamber was adjusted by mixing a stream of dry N_2 and another of water-saturated N_2 at controlled flow rates. The RH and temperature were recorded by the T & RH meter (Centertek Center 310, ±2.5% RH and ±0.7 °C).

Apparatus and Conditions for the Measurements. The experimental setup and conditions used in this work are identical to those in Wang's study.[28] Figure 1 shows the schematic diagram of the experimental setup. The Renishaw InVia confocal Raman spectrometer was used to obtain the Raman spectra. A 514.5 nm Ar^+ laser (LS-514 model, Laserphysics) was employed as an excitation source. With the pinhole-in mode, the laser beam was focused on the sample in a diameter of about 1 μm and produced the backscattering signal with the 50× objective of the Leica DMLM microscope. After passing through a 1800 g/mm grating, the backscattering signal was detected by the charge-coupled device (CCD) with a spectral resolution of about 1 cm^{-1}. A 514.5 nm notch filter was adopted to remove the strong Rayleigh scattering. The output power of the laser was adjusted to 20 mW. The spectra in the range of 200−4000 cm^{-1} were accumulated five times by scanning the grating, each time with an exposure time of 10 s. Spectral calibration was made with the silicon band of 520 ± 0.05 cm^{-1} as standard before the experiment. To ensure that the samples in the chamber could equilibrate with the ambient humidity, about 30 min was spent before the spectral measurement at each given RH value. All the measurements were made at ambient temperature of 22−24 °C. All the spectra with a reproducibility of 0.2 cm^{-1} were obtained by the Wire 2.0 program offered by Renishaw. The photographs of the $NaNO_3$ particles were obtained by the Leica DMLM microscope in the deliquescence processes.

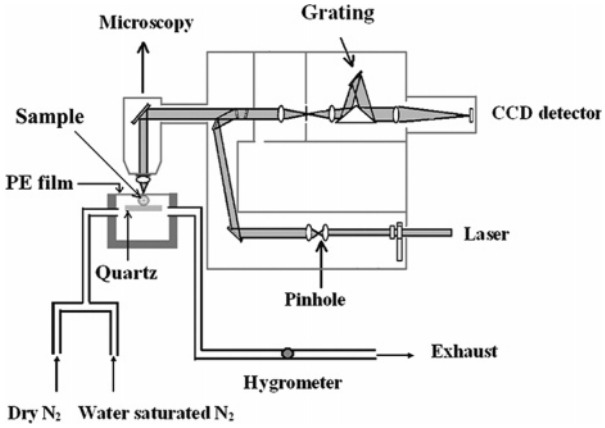

Figure 1. Schematic diagram of the experimental setup for the micro-Raman observations of $NaNO_3$ particles on a quartz substrate.

Results and Discussion

Raman Spectra of $NaNO_3$ Droplets with Different WSRs. The bulk nitrate solutions have been extensively investigated by various means.[29−34] In this work, supersaturated $NaNO_3$ droplets on the substrate were obtained, benefiting from the relaxation of the saturation constraint in the water evaporation processes. Larger $NaNO_3$ droplets were found to easily crystallize in the supersaturated state not far from the saturation point (WSR = 5.2 at 74.5% RH),[12,24] while smaller droplets usually achieved highly supersaturated states rather than being crystallized at low RHs. Considering that larger droplets can provide Raman spectra with higher quality, we selected droplets with a diameter of ∼100 μm to obtain the spectra at high RHs. Once the larger droplets crystallized, we had to search for smaller ones to acquire the Raman spectra of the highly concentrated $NaNO_3$ droplets. The smallest droplet had a diameter of ∼10 μm, which did not crystallize until the RH was lower than 29.5% (WSR = 1.0). Thus, we successfully obtained the Raman spectra of $NaNO_3$ droplets with WSRs from 7.6 to 1.0 (82.0−29.5% RH) as shown in Figure 2. For comparison, Raman spectra of a 1.0 mol dm^{-3} $NaNO_3$ solution are also displayed at the top of this figure. All the spectra are normalized with the intensity of the $\nu_1(NO_3^-)$ band as the standard. It is striking that the spectra of the larger droplets (WSR ≥ 3.2) show S/N ratios at the same level as those of the bulk solution. Even for smaller droplets (WSR ≤ 1.9), the Raman spectra are good enough to provide reliable structural information on the supersaturated $NaNO_3$ droplets.

For the 1.0 mol dm^{-3} $NaNO_3$ solution, the $\nu_1(NO_3^-)$ band is centered at ∼1048 cm^{-1} with approximately symmetric shape. The $\nu(H_2O)$ band is composed of two components: a main peak at ∼3437 cm^{-1} and a shoulder at ∼3256 cm^{-1}. For $NaNO_3$ droplets, the $\nu_1(NO_3^-)$ band continuously blue shifts and apparently broadens with a decrease of WSR. It appears at

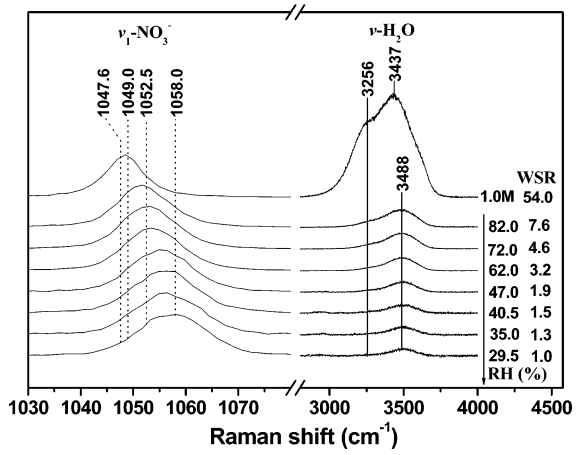

Figure 2. Raman spectra of the $NaNO_3$ droplets at various RHs in the efflorescence process. The top one is the Raman spectrum of a 1.0 mol dm^{-3} $NaNO_3$ solution. (The WSRs are obtained from refs 12 and 24.)

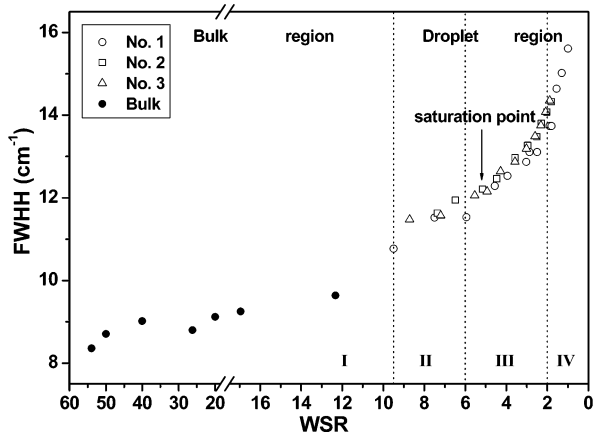

Figure 3. fwhh of the $\nu_1(NO_3^-)$ band of the bulk $NaNO_3$ solutions and the $NaNO_3$ droplets with various WSRs (three sets of data for the droplets and one set of data for the bulk solutions).

$\sim$1058 cm^{-1} when WSR reaches 1.0. The $\nu(H_2O)$ band is much weaker than that of the 1.0 mol dm^{-3} $NaNO_3$ solution. Besides, the $\nu(H_2O)$ band shows a main peak at $\sim$3488 cm^{-1}, which remains almost immovable with decreasing WSR. The shoulder at $\sim$3256 cm^{-1} becomes fairly weak but can still be resolved even at WSR = 1.0.

***$\nu_1(NO_3^-)$* Bands of the $NaNO_3$ Droplets.** In the bulk $NaNO_3$ solutions, ion pairs between Na^+ and NO_3^- have been disclosed with the Raman spectroscopic technique.[31−34] The formation of ion pairs evidently altered the width and frequency of the $\nu_1(NO_3^-)$ band.[32,33] Na^+ was found to very easily form ion pairs with NO_3^- even when the concentration was below 3 mol dm^{-3}.[33] Selecting $NaNO_3$ droplets as the object, we can extend Raman observation into the supersaturation area with a WSR as low as 1.0, which cannot be performed in bulk solutions.

Figure 3 displays the full width at half-height (fwhh) of the $\nu_1(NO_3^-)$ band as a function of WSR, including the results from bulk solutions with WSRs of 54.0−12.3 and those from droplets with WSRs of 9.5−1.0. In the WSR range from 54.0 to 1.0, the graph can be roughly divided into four regions with three boundaries, i.e., WSR = 9.5, WSR = 6.0, and WSR = 2.0. The fwhh is not very sensitive to the WSR variation for the bulk $NaNO_3$ solutions in region I; namely, it slightly increases from 8.4 to 9.7 cm^{-1} in the wide WSR range from 54.0 to 12.3. In region II for droplets with WSRs of 9.5−6.0, the gradient of the fwhh−WSR curve has an apparent increase. In region III

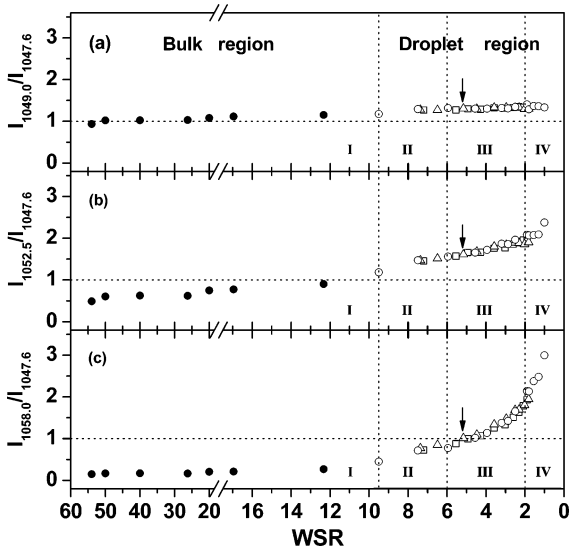

Figure 4. (a) $I_{1049.0}/I_{1047.6}$, (b) $I_{1052.5}/I_{1047.6}$, and (c) $I_{1058.0}/I_{1047.6}$ of the $NaNO_3$−H_2O system against WSR. The saturation point is indicated by an arrow.

of WSRs from 6.0 to 2.0, the fwhh is sensitive to the change of WSR, increasing from 12.1 to 14.1 cm^{-1}. In region IV with WSR < 2.0, the fwhh rapidly increases with the decline of WSR and finally reaches $\sim$15.6 cm^{-1} at WSR = 1.0.

In bulk $NaNO_3$ solutions with WSR = 54.0−12.3, NO_3^- anions mostly exist as SIPs (solvent-separated ion pairs) according to the band-component analysis.[32] At the same time, both the peak position and the fwhh for the $\nu_1(NO_3^-)$ band of SIPs (1049.0 and 3.55 cm^{-1}) are similar to those of free NO_3^- ions (1047.6 and 3.40 cm^{-1}).[32] As a result, the formation of SIPs only induces a small increase of fwhh in region I. In region II, plenty of CIPs appear, showing a band at 1052.5 cm^{-1} with a large fwhh (8.11 cm^{-1}).[32] The increased fwhh for CIPs is virtually induced by the long-range environmental perturbation, which makes the vibrational relaxation decrease from ca. 1 to 0.65 ps.[32] Therefore, the fwhh dominated by the CIPs apparently increases in region II. In region III with WSR = 6.0−2.0, the marked increase of fwhh very likely implies the appearance of new associated species, i.e., complicated CIPs with bidentate and bridged bidentate structures. In region IV of WSR < 2.0, the pronounced increase of fwhh should be assigned to the quick increase of complicated CIPs.

Through band-component analysis, the $\nu_1(NO_3^-)$ bands of free NO_3^- ions, SIPs, and CIPs were resolved at 1047.6, 1049.0, and 1052.5 cm^{-1}, respectively.[32] In the present work, the maximum position of the $\nu_1(NO_3^-)$ envelope blue shifts to $\sim$1058 cm^{-1} for the extremely supersaturated droplet (WSR = 1.0). The intensity at 1058 cm^{-1} should mainly arise from CIPs with complicated structures. On these bases, the relative proportion of each species can be roughly estimated on the basis of the intensity at the corresponding position.

Figure 4 describes the intensity ratios $I_{1049.0}/I_{1047.6}$ (a), $I_{1052.5}/I_{1047.6}$ (b), and $I_{1058.0}/I_{1047.6}$ (c) as a function of WSR. Each of these curves is divided into four regions, corresponding to those in Figure 3. The boundaries of WSR = 9.5 and WSR = 6.0 are pertinent to vast formations of CIPs and complicated CIPs, respectively. Because the $\nu_1(NO_3^-)$ band of the SIPs is very close to that of the free NO_3^-, the value of $I_{1049.0}/I_{1047.6}$ shows no distinct transition in the whole WSR range from 54.0 to 1.0 as displayed in Figure 4a. In Figure 4b,c, however, the intensity ratios vary sensitively with the WSR variation. In region I with WSRs between 54.0 and 12.3 (bulk solution area), there is an

order of $1 > I_{1052.5}/I_{1047.6} > I_{1058.0}/I_{1047.6}$, indicating that the free NO_3^- anions and SIPs dominate in the solutions. In region II ($9.5 > WSR > 6.0$), the order of $I_{1052.5}/I_{1047.6} > 1 > I_{1058.0}/I_{1047.6}$ implies that the CIPs account for the largest proportion. In region III of WSR = 6.0−2.0, the curve shows a slow increase in Figure 4b but a rapid increase in Figure 4c. At WSR = 2.0, the value of $I_{1058.0}/I_{1047.6}$ catches up with that of $I_{1052.5}/I_{1047.6}$, both of them reaching about 2.0. This indicates that the complicated CIPs quickly increase when WSR is below 6.0 and become the main component in region IV with WSR < 2.0. Such component conversion is in accordance with the apparent blue shift of the $\nu_1(NO_3^-)$ envelope with the decrease of RH in Figure 2. Similarly, Irish et al. observed that the $\nu_1(NO_3^-)$ band shifted from 1049 ± 0.5 cm^{-1} for dilute alkali-metal nitrates including KNO_3, $CsNO_3$, and $LiNO_3$ to higher frequencies for their concentrated solutions.[31] In particular, the notably high frequency (1054 cm^{-1}) for $\nu_1(NO_3^-)$ appeared in the Raman spectrum of a very concentrated $LiNO_3$ solution (9.02 mol dm^{-3}), which was ascribed to the formation the CIPs. The blue shift induced by the formation of the ion pair can be further comprehended on the basis of the decrease of the effective mass of the vibrating units (the oxygen atoms in the case of nitrate) caused by the disruption of the hydrogen bonds between NO_3^- and H_2O.[33]

The conclusion that large numbers of CIPs between Na^+ and NO_3^- are formed at WSR = 9.5 is consistent with hydration numbers of 3−6 for Na^+ and 3 for NO_3^-.[35,36] From the dynamic point of view, it is favorable for NO_3^- to enter into the first coordination layer of Na^+ since the residence time of hydrated water molecules of Na^+ ($(9.9 \pm 0.3) \times 10^{-12}$ s) is very similar to that of pure water ($(4.6 \pm 0.3) \times 10^{-12}$ s).[37]

Water Stretching Vibration Band. For pure liquid water, the O−H stretching envelope was generally considered to be composed of four components, an icelike component (C_1) at ~3230 cm^{-1}, an icelike liquid component (C_2) at ~3420 cm^{-1}, a liquidlike amorphous phase (C_3) at ~3540 cm^{-1}, and monomeric water molecules (C_4) at ~3620 cm^{-1}.[11,37,38] The addition of ions will change the contour of the O−H stretching band because of their effects on the hydrogen-bonding structures between water molecules.[9,37,39] For Na^+ with a low charge-to-radius ratio, there is little difference between its hydrated water molecules and the bulk water molecules from the dynamic point of view.[35] Hence, Na^+ does not obviously influence the O−H stretching vibration, which was also proved by means of low-frequency Raman scattering and femtosecond pump−probe spectroscopy.[40,41] However, NO_3^- anion with a plane structure has a strict requirement for the orientation of the water molecules associated with it.[37] Consequently, the ionic hydration of NO_3^- will strongly destroy the three-dimensional network structures of water molecules.

The half-ellipsoidal $NaNO_3$ droplets on the quartz substrate have the advantages of achieving the supersaturated state and avoiding the MDR disturbance. Thus, authentic O−H stretching bands of water molecules in supersaturated $NaNO_3$ solutions were obtained as shown in Figure 2. The main peak arises at ~3488 cm^{-1}, presenting the interactions of water molecules with NO_3^-.[37] Besides, a shoulder appears at ~3256 cm^{-1}, which can be ascribed to the water molecules hydrogen-bonding with their four neighboring water molecules.[37] Even in the extremely supersaturated $NaNO_3$ droplets with a WSR of 1.0 (29.5% RH), the shoulder at ~3256 cm^{-1} can be resolved, indicating a small amount of water molecules still tend to form fully hydrogen-bonding five-molecule tetrahedral structures. A similar phenomenon was also observed in the supersaturated $NaClO_4$ solution.[9] This can be anticipated because the residence time of the hydrated water molecules of Na^+ is close to that of bulk water molecules.[37]

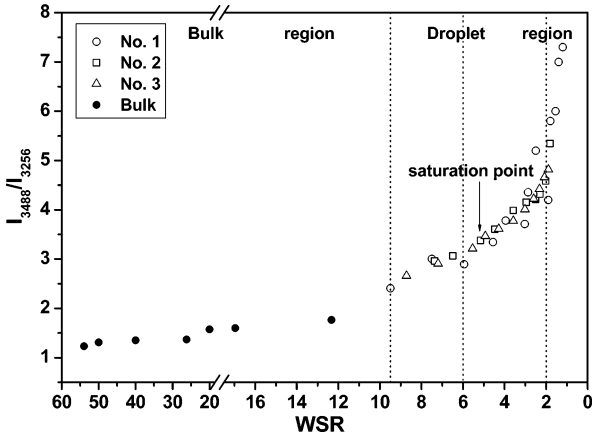

Figure 5. Intensity ratio of I_{3488}/I_{3256} as a function of WSR (three sets of data for the droplets and one set of data for the bulk solutions).

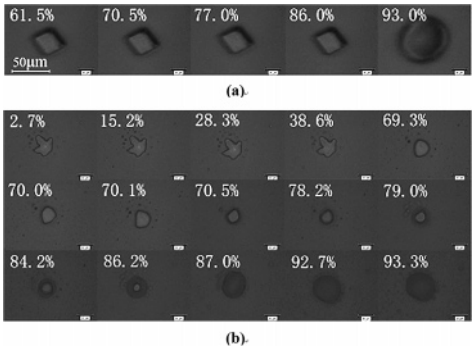

Figure 6. Morphological changes of solid $NaNO_3$ particles with (a) rhombohedral shape and (b) maple leaf shape in the deliquescence processes.

More structural information can be drawn from the evolution of I_{3488}/I_{3256}, the ratio of the weak hydrogen-bonding components to the strong ones, which is presented in Figure 5. For bulk $NaNO_3$ solutions, the values of I_{3488}/I_{3256} slightly increase from 1.3 (WSR = 54) to 1.8 (WSR = 12.3). For $NaNO_3$ droplets, they vary from 2.5 (WSR = 9.5) to 4.7 (WSR = 2.0) and finally to 7.3 (WSR = 1.0). When CIPs are formed, the strong hydrogen-bonding components are strictly depressed according to the remarkable increase of I_{3488}/I_{3256}.

Morphology-Dependent Deliquescence. Generally, regular single crystals could be obtained by slowly evaporating large $NaNO_3$ droplets at RH slightly lower than the saturation point (74.5% RH). Small $NaNO_3$ droplets usually retained the liquid state far below the saturation RH. Efflorescence of the small $NaNO_3$ droplets in the supersaturation region often produced irregular solid particles with rough surfaces. To understand the morphology effect on the deliquescence process, photographs of two types of solid $NaNO_3$ particles at various RHs were obtained as shown in Figure 6. In Figure 6a, the rhombohedron-shaped $NaNO_3$ single crystal with smooth surfaces remains unchanged in the region of RH < 86.0% rather than being dissolved at the reported deliquescence point of 74.5% RH (25 °C).[12,24] At 93% RH, the particle grows into a solution droplet, indicating that it sharply takes up plenty of water in the RH region of 86.0−93.0%. On the contrary, the maple-leaf-shaped $NaNO_3$ particle in Figure 6b experiences a continuous morphology change when the RH stays at ~70.0%. The edges and corners become smoother with increasing equilibration time. We propose that the surface should be covered by a thin layer

of initially adsorbed water with etching ability even though it cannot be confirmed with the optical microscope. With further increasing RH, the particle slowly absorbs water from the ambient, resulting in a slightly thicker water layer at ~79.0% RH, which can be resolved with the Leica DMLM microscope. In spite of the noticeable morphology changes, the particle does not completely deliquesce to a solution droplet within a long period of time (about 1 h) at about 79.0% RH. Upon an increase of RH from ~79.0% to ~86.0%, the water layer on the particle surface obviously thickens. However, the adsorbed water hardly increases with an extension of the equilibration time at a given RH. Eventually, the particle is completely dissolved at 92.7% RH, then continues to absorb water, and bloats with increasing RH.

The complicated morphology changes of the irregular particle in Figure 6b may contain much information about the physical and chemical properties of the rough surfaces. Similar phenomena were also observed by Dai et al.[42] They discovered that the NaCl (100) surfaces with numerous atomic steps were covered with water even at humidity far below the deliquescence point.[42] The step edges and surface defects with higher surface energy absorbed water prior to deliquescence, resulting in surface arrangement due to the diffusion of the hydrated Na^+ and Cl^- on the surface.[43] Therefore, the morphology changes in Figure 6b could be attributed to the initially adsorbed water, which can accelerate the ionic mobility on the particle surface and lead to the recrystallization as well as the regularity on the surface.[19,26,44,45] We will discuss two kinds of surface water, i.e., residual water and initially adsorbed water on the rough $NaNO_3$ particle surface, in section 5 on surface-sensitive Raman spectroscopy.

On the other hand, water uptake at RHs slightly below the deliquescence point was also discovered for polycrystalline $(NH_4)_2SO_4$ and $(NH_4)_3HSO_4$ aerosol particles by Colberg et al.[46] They introduced the concept of predeliquescence to designate this phenomenon. The predeliquescence for polycrystalline samples obtained through evaporating solution was previously forecasted by Cantrell et al.[47] Therefore, the morphology changes in Figure 6b at RH slightly lower than the deliquescence point of $NaNO_3$ particles are somewhat related to the predeliquescence process of the maple-leaf-shaped $NaNO_3$ particle.

It is interesting to notice that both the regular rhombohedron-shaped $NaNO_3$ particle and maple-leaf-shaped $NaNO_3$ particle are ultimately dissolved at ~93% RH, much higher than the deliquescence point observed by Tang.[12,24] Similarly, Cantrell et al. found that deliquescence of a single crystal of NaCl was at 86% RH, showing a large delay compared with the saturation point of NaCl solution (75% RH).[47] Moreover, they found that the NaCl particles annealed by exposure to RHs slightly below the saturation point showed a larger spread in the values of deliquescence RH. They assigned the hysteretic deliquescence to nucleated deliquescence, which was ascribed to the low density of defects on the particles.[47,48] We believe that the predeliquescence in our experiment plays the role of annealing; that is, it reduces the density of defects on the irregular solid particle.

Spectroscopic Evidence for Residual Water and the Initially Adsorbed Water. Raman spectra of the two types of $NaNO_3$ particles were obtained at various RHs, which are shown in parts a and b, respectively, of Figure 7. All the spectra are normalized with the intensity of the $\nu_1(NO_3^-)$ band as the standard.

For the $NaNO_3$ particle with rhombohedral shape, the sharp $\nu_1(NO_3^-)$ peak appears at 1068 cm^{-1} as a characteristic of a

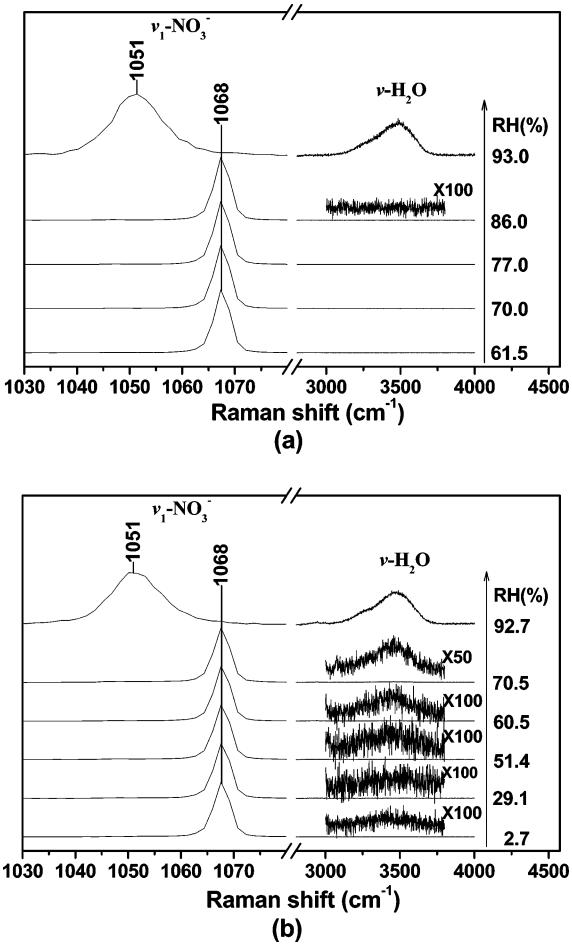

Figure 7. Raman spectra of solid $NaNO_3$ particles with (a) rhombohedral shape and (b) maple leaf shape at various RHs in the deliquescence processes.

$NaNO_3$ crystal at an RH of 61.5−86.0%. Correspondingly, no signal of water molecules can be observed even though the line intensity in the $\nu(H_2O)$ region (3000−3800 cm^{-1}) is multiplied by 100 at 86.0% RH. At 93.0% RH, the $\nu_1(NO_3^-)$ band broadens and red shifts to 1051 cm^{-1} accompanied by the increase of the $\nu(H_2O)$ band. Such spectral evolutions are consistent with the morphological changes in Figure 6a, indicating that the $NaNO_3$ particle with rhombohedral shape takes up enough water and is transformed into the liquid state at 93.0% RH. For the maple-leaf-shaped $NaNO_3$ particle in Figure 7b, the $\nu_1(NO_3^-)$ band changes similarly to that in Figure 7a. It remains at 1068 cm^{-1} as the RH increases from 2.7% to 70.5% and then red shifts to 1051 cm^{-1} at 92.7% RH. However, the weak but significant $\nu(H_2O)$ band can be observed even at 2.7−60.5% RH. Interestingly, the $\nu(H_2O)$ bands at RHs of 51.4% and 60.5% are somewhat stronger than those at RHs of 2.7% and 29.1%. At 70.5% RH, a visible strengthening of the $\nu(H_2O)$ band is detected. At 92.7% RH, the $\nu(H_2O)$ band becomes fairly strong as a result of the complete deliquescence.

The spectral evolutions in Figure 7b provide knowledge on residual water and the initially adsorbed water on the surface of the maple-leaf-shaped $NaNO_3$ particle on the molecular level. When RH is lower than about 70%, the particle seems not to absorb water from the ambient since its shape does not change. Thus, the resolved weak $\nu(H_2O)$ band in 2.7−60.5% RH is a characteristic of residual water. As for the slight intensity difference for the $\nu(H_2O)$ band in the RH range of 2.7−60.5%, a possible reason should be taken into consideration. That is, there are different amounts of residual water at the positions

for each measurement since the particle is focused in a diameter of only about 1 μm. In other words, the residual water should be surface water (adhering to the particle surface) or agglomerate water (agglomerated at the defective sites) but did not homogeneously disperse inside the particle.[49] Such kinds of water molecules were also found on the $Ca(NO_3)_2$ particles even at very low RH.[8,19,44] They can powerfully promote the particles to react with some gases in air, such as, HNO_3, $ClONO_2$, and N_2O_5,[50−53] which have important atmospheric implications.[26]

On the other hand, the distinctly increased intensity of the $\nu(H_2O)$ band at 70.5% RH suggests the appearance of the initially adsorbed water on the particle. That is to say, the irregular particle does begin to take up water from the ambient at ∼70.0% RH probably induced by residual water which interacts with the gas phase.[46] These initially adsorbed water molecules dissolve a small amount of $NaNO_3$ to form a thin solution film, wrapping the undissolved solid core inside. Accompanied by the reduction of the solid core, the solution layer thickens with increasing RH but hardly changes with extension of the equilibration time at a certain RH. Consequently, the particle finally completely deliquesces in the RH region of about 86−93%.

Conclusions

The $NaNO_3$−H_2O system from a dilute solution (WSR = 54.0) to an extremely supersaturated droplet (WSR = 1.0) on the quartz substrate has been investigated by means of confocal Raman spectroscopy. It can be concluded that free NO_3^- and solvent-separated ion pairs are dominative in bulk $NaNO_3$ solutions with WSR = 54.0−12.3. For $NaNO_3$ droplets with WSR = 9.5−6.0, a large proportion of contact ion pairs between Na^+ and NO_3^- are formed, inducing obvious increases of fwhh and the frequency of the $\nu_1(NO_3^-)$ envelope. By further decreasing the WSR for the $NaNO_3$ droplets, diverse contact ion pairs with complicated structures abruptly increase. In the region of WSR < 2.0, the complicated contact ion pairs account for the largest proportion of total association species, which are characterized by the noticeable large fwhh and high frequency of the $\nu_1(NO_3^-)$ envelope. The hydrogen-bonding structures of water molecules mainly depend on the $NaNO_3$ concentrations, especially in the supersaturation area.

The deliquescence behavior of a solid $NaNO_3$ particle is morphology-dependent. A regular $NaNO_3$ particle with a rhombohedral shape suddenly absorbs water and turns into a solution droplet at an RH of 86−93%. However, a maple-leaf-shaped $NaNO_3$ particle starts to slowly take up water at ∼70% RH due to the residual water on the rough surface. The recrystallization caused by the initially adsorbed water results in a regular solid core swathed in a thin solution layer. The deliquescence RH of the maple-leaf-shaped $NaNO_3$ particle is also 86−93%, which is similar to the case of the $NaNO_3$ particle with a rhombohedral shape.

Acknowledgment. This work was supported by the NSFC (Grants 20073004, 20473012, and 20673010), and the Trans-Century Training Program Foundation for the Talents by the Ministry of Education of China is also gratefully acknowledged.

References and Notes

(1) Orr, C., Jr.; Hurd, F. K.; Corbett, W. J. *J. Colloid Sci.* **1958**, *13*, 472.
(2) Martin, S. T. *Chem. Rev.* **2000**, *100*, 3403.
(3) Choi, M. Y.; Chan, C. K. *J. Phys. Chem. A* **2005**, *109*, 1042.
(4) Dougherty, R. C. *J. Phys. Chem. B* **2001**, *105*, 4514.
(5) Rakitin, A. R.; Pack, G. R. *J. Phys. Chem. B* **2004**, *108*, 2712.
(6) Mudi, A.; Chakravarty, C. *J. Phys. Chem. B* **2006**, *110*, 8422.
(7) Zhang, Y. H.; Chan, C. K. *J. Phys. Chem. A* **2000**, *104*, 9191.
(8) Zhang, Y. H.; Chan, C. K. *J. Phys. Chem. A* **2002**, *106*, 285.
(9) Zhang, Y. H.; Chan, C. K. *J. Phys. Chem. A* **2003**, *107*, 5956.
(10) Wang, L. Y; Zhang, Y. H.; Zhao, L. J. *J. Phys. Chem. A* **2005**, *109*, 609.
(11) Zhang, Y. H.; Choi, M. Y.; Chan, C. K. *J. Phys. Chem. A* **2004**, *108*, 1712.
(12) Tang, I. N.; Fung, K. H. *J. Chem. Phys.* **1997**, *106*, 1653.
(13) Mitchem, L.; Buajarern, J.; Hopkins, R. J.; Ward, A. D.; Gilham, R. J. J.; Johnston, R. L.; Reid, J. P. *J. Phys. Chem. A* **2006**, *110*, 8116.
(14) Reid, J. P.; Mitchem, L. *Annu. Rev. Phys. Chem.* **2006**, *57*, 245.
(15) Hopkins, R. J.; Reid, J. P. *J. Phys. Chem. B* **2006**, *110*, 3239.
(16) Mitchem, L.; Buajarern, J.; Ward, A. D.; Reid, J. P. *J. Phys. Chem. B* **2006**, *110*, 13700.
(17) Wood, B. R.; Heraud, P.; Stojkovic, S.; Morrison, D.; Beardall, J.; McNaughton, D. *Anal. Chem.* **2005**, *77*, 4955.
(18) Keene, W. C.; Sander, R.; Pszenny, A. A. P.; Vogt, R.; Crutzen, P. J.; Galloway, J. N.; et. al. *J. Aerosol Sci.* **1998**, *29*, 339.
(19) Weis, D. D.; Ewing, G. E. *J. Phys. Chem. A* **1999**, *103*, 4865.
(20) Tolocka, M. P.; Saul, T. D.; Johnston, M. V. *J. Phys. Chem. A* **2004**, *108*, 2659.
(21) Robbins, R. C.; Cadle, R. D.; Eckhardt, D. L. *J. Meteorol.* **1959**, *16*, 53.
(22) Hemminger, J. C. *Int. Rev. Phys. Chem.* **1999**, *18*, 387.
(23) Zhao, L. J.; Zhang, Y. H.; Wei, Z. F.; Cheng, H.; Li, X. H. *J. Phys. Chem. A* **2006**, *110*, 951.
(24) Tang, I. N.; Munkelwitz, H. R. *J. Geophys. Res.* **1994**, *99*, 18801.
(25) Lee, C. T.; Hsu, W. C. *J. Aerosol Sci.* **2000**, *31*, 189.
(26) Gysel, M.; Weingartner, E.; Baltensperger, U. *Environ. Sci. Technol.* **2002**, *36*, 63
(27) Hoffman, R. C.; Laskin, A.; Finlayson-Pitts, B. *J. Aerosol Sci.* **2004**, *35*, 869.
(28) Wang, F.; Zhang, Y. H.; Li, S. H.; Wang, L. Y.; Zhao, L. J. *Anal. Chem.* **2005**, *77*, 7148.
(29) Waterland, M. R.; Kelley, A. M. *J. Chem. Phys.* **2000**, *113*, 6760.
(30) Waterland, M. R.; Stochwell, D.; Kelley, A. M. *J. Chem. Phys.* **2001**, *114*, 6249.
(31) Irish, D. E.; Davis, A. R. *Can. J. Phys.* **1968**, *46*, 943.
(32) Frost, R. L.; James, D. W. *J. Chem. Soc., Faraday Trans.* **1982**, *78*, 3249.
(33) Vollmar, P. M. *J. Chem. Phys.* **1963**, *39*, 2236.
(34) Spohn, P. D.; Brill, T. B. *J. Phys. Chem.* **1989**, *93*, 6224.
(35) White, J. A.; Schwegler, E.; Galli, G.; Gygi, F. *J. Chem. Phys.* **2000**, *113*, 4668.
(36) Wang, X. B.; Wang, L. S. *J. Chem. Phys.* **2002**, *116*, 561.
(37) Liu, J. H.; Zhang, Y. H.; Wang, L. Y.; Wei, Z. F. *Spectrochim. Acta, Part A* **2005**, *61*, 893.
(38) Walrafen, G. E. *J. Chem. Phys.* **1970**, *52*, 4176.
(39) Wei, Z. F.; Zhang, Y. H.; Zhao, L. J.; Liu, J. H.; Li, X. H. *J. Phys. Chem. A* **2005**, *109*, 1337.
(40) Omta, A. W.; Kropman, M. F.; Woutersen, S.; Bakker, H. J. *Science* **2003**, *301*, 347.
(41) Wang, Y.; Tominaga, Y. *J. Chem. Phys.* **1994**, *101*, 3453.
(42) Dai, Q.; Hu, J.; Salmeron, M. *J. Phys. Chem. B* **1997**, *101*, 1994.
(43) Moffat, J. B.; McIntosh, R. *Can. J. Chem.* **1957**, *35*, 1511.
(44) Karlsson, R.; Ljungstrom, E. *J. Aerosol Sci.* **1995**, *26*, 39.
(45) Zangmeister, C. D.; Pemberton, J. E. *J. Phys. Chem. B* **1998**, *102*, 8950.
(46) Colberg, C. A.; Krieger, U. K.; Peter, T. *J. Phys. Chem. A* **2004**, *108*, 2700.
(47) Cantrell, W.; McCrory, C.; Ewing, G. E. *J. Chem. Phys.* **2002**, *116*, 2116.
(48) Djikaev, Y. S.; Bowles, R.; Reiss, H.; Hämeri, K.; Laaksonen, A.; Väkevä, M. *J. Phys. Chem. B* **2001**, *105*, 7708.
(49) Vogt, R.; Finlayson-Pitts, B. J. *J. Phys. Chem.* **1994**, *98*, 3747.
(50) Wan, J. K. S.; Pitts, J. N., Jr.; Beichert, P.; Finlayson-Pitts, B. J. *Atmos. Environ.* **1996**, *30*, 3109.
(51) Peters, S. J.; Ewing, G. E. *J. Phys. Chem.* **1996**, *100*, 14093.
(52) Langer, S.; Pemberton, R. S.; Finlayson-Pitts, B. J. *J. Phys. Chem. A* **1997**, *101*, 1277.
(53) Laux, J. M.; Hemminger, J. C.; Finlayson-Pitts, B. J. *Geophys. Res. Lett.* **1994**, *21*, 1623.